Title

Hitching a Ride: Mechanics of Transport Initiation through Linker-Mediated Hitchhiking

Journal

Biophysical Journal, 118(6)

ISSN

0006-3495

Authors

Mogre, Saurabh S
Christensen, Jenna R
Niman, Cassandra S
et al.

Publication Date

2020-03-01

DOI

10.1016/j.bpj.2020.01.024

Peer reviewed

Manuscript submitted to **Biophysical***Journal*
Article

Hitching a Ride: Mechanics of Transport Initiation Through Linker-Mediated Hitchhiking

S. S. Mogre[1], J. R. Christensen[2], C. S. Niman[3], S. L. Reck-Peterson[2,4,5], and E. F. Koslover[1,*]

[*]Correspondence: ekoslover@ucsd.edu

ABSTRACT In contrast to the canonical picture of transport by direct attachment to motor proteins, recent evidence shows that a number of intracellular 'cargos' navigate the cytoplasm by hitchhiking on motor-driven 'carrier' organelles. We describe a quantitative model of intracellular cargo transport via hitchhiking, examining the efficiency of hitchhiking initiation as a function of geometric and mechanical parameters. We focus specifically on the parameter regime relevant to the hitchhiking motion of peroxisome organelles in fungal hyphae. Our work predicts the dependence of transport initiation rates on the distribution of cytoskeletal tracks and carrier organelles, as well as the number, length and flexibility of the linker proteins that mediate contact between the carrier and the hitchhiking cargo. Furthermore, we demonstrate that attaching organelles to microtubules can result in a substantial enhancement of the hitchhiking initiation rate in tubular geometries such as those found in fungal hyphae. This enhancement is expected to increase the overall transport rate of hitchhiking organelles, and lead to greater efficiency in organelle dispersion. Our results leverage a quantitative physical model to highlight the importance of organelle encounter dynamics in non-canonical intracellular transport.

SIGNIFICANCE A variety of cellular components are transported via hitchhiking by attaching to other motile organelles. Defects in the molecular machinery responsible for organelle hitchhiking may be linked with neurodegenerative disorders. To date, no comprehensive physical models of this non-canonical mode of transport have been developed. In particular, the connection between molecular- and organelle-scale properties of hitchhiking components and their effect on cellular-scale transport has remained unclear. Here, we investigate the mechanics of hitchhiking initiation and explore organelle interactions that can modulate the efficiency of this process.

INTRODUCTION

Regulated movement of proteins, vesicles, and organelles plays an important role in the growth, metabolism and maintenance of cellular health. These particles move within a crowded and dynamic intracellular environment, aided by a dedicated transport machinery that typically comprises molecular motor proteins walking upon a network of cytoskeletal filaments. Precise control of transport ranging over length scales from a few microns to tens of centimeters is achieved by regulating the interactions between moving and stationary cargo, motors, and other cytoskeletal structures. Defects in the regulation of organelle movement can lead to pathologies, particularly in long cells such as neurons, where axonal transport deficiencies have been implicated in neurodegenerative disorders including Alzheimer's, amyotrophic lateral sclerosis (ALS), and multiple sclerosis(1–3).

The traditional picture of intracellular transport involves the direct attachment of cargo to adaptor proteins that recruit cytoskeletal motors, which carry the cargo processively along microtubule tracks(4–6). However, recent experimental evidence suggests that a variety of cargos such as peroxisomes, lipid droplets, messenger ribonucleoprotein (mRNP) complexes, RNA granules and the endoplasmic reticulum can attach to other motile organelles, and navigate the cytoplasm through a mode of transport known as "hitchhiking"(7–15). Hitchhiking is characterized by the presence of a motor-driven "carrier" organelle which is required for processive transport of a cargo (the hitchhiker). Specifically, organelle hitchhiking has been defined as conforming to three criteria: 1) long-range co-migration of cargo and carrier organelles, 2) lack of membrane fusion between distinct cargo and carrier particles, and 3) cargo transport is dependent on carrier movement, while carriers can move independently of cargo(16). The ubiquity of hitchhiking cargos across systems suggests that this is a broadly applicable transport mechanism, whose efficiency may dictate the distribution and delivery of particles that are critical for optimal cellular function.

Previous theoretical models of canonical microtubule-based transport have focused on the distribution of cytoskeletal tracks(17), interplay between diffusive and processive transport (18, 19), characteristics of motor processivity and turning (20), and cargo behavior at microtubule intersections(21, 22).

The non-canonical hitchhiking mechanism, however, is governed by fundamentally different interactions at the molecular and organelle level, as compared to classic motor-driven transport. The physical principles that underlie hitchhiking efficiency have not yet been quantitatively explored.

Although the molecular components of hitchhiking have yet to be fully identified for many cargos, linker proteins which link the hitchhiking cargo to the carrier organelle have been identified in some cases(15, 16). For example, in the filamentous fungus *Ustilago maydis*, mRNAs and their associated polysomes attach to early endosomes via an interaction between RNA-binding protein Rrm4 and early endosome-associated protein Upa1 (7–10). In both *Ustilago maydis* and *Aspergillus nidulans*, another filamentous fungus, peroxisomes hitchhike on early endosomes (12, 13). In *Aspergillus*, the protein PxdA is required for peroxisome hitchhiking(13), and is a putative linker between early endosomes and peroxisomes. In rat neurons, RNA granules hitchhike on motile lysosomes using the ALS-associated protein Annexin A11 as a linker(15). While such linker proteins have been shown to be required for hitchhiking in these circumstances, it remains unknown how their mechanical and structural properties modulate hitchhiking efficiency.

In some cell types, organelles such as peroxisomes and mitochondria have been observed to attach to microtubules when not being actively transported(23–25). Such tethering allows for regulated placement of organelles within the cell(25–28). Tethering may also enhance the ability of cargo to interact with the transport machinery, increasing the rate of initiating active runs while restricting short-range diffusion(19). Peroxisomes in particular have been found to exhibit both diffusive motion and microtubule tethering depending on cell type and context (14, 23), indicating that both modes of motion may play a role in organelle motility. Here, we explore how tethering to microtubule tracks can enhance the rate of transport initiation for hitchhiking cargos, by placing them within easy reach of passing carrier organelles.

Given the complexity of intracellular transport processes, many studies of transport have focused on the simplified geometries found in long cylindrical cellular projections(13, 14). Such projections feature polarized arrays of parallel microtubules, with few intersections and essentially one-dimensional movement of cargo. Neuronal axons and the hyphae of filamentous fungi exhibit a similar cylindrical geometry. Filamentous fungi such as *Aspergillus nidulans* are particularly amenable to genetic manipulation and imaging, providing convenient experimental systems for studies of intracellular transport (29).

Linearly extended cellular systems such as axons and hyphae generally require efficient transport machinery to maintain a well-dispersed distribution of organelles. This distribution is determined both by the site of organelle biogenesis and by the transport machinery available to spread organelles away from these sites. In the filamentous fungus *Penicillium chrysogenum* peroxisome generation occurs preferentially at the hyphal tip(30). In *Ustilago maydis*, an actin-dependent slow polar drift has been demonstrated to result in an accumulation of peroxisomes at the hyphal tip in the absence of hitchhiking transport(14). In both cases, the hyphae are sufficiently long (on the order of 40μm from the last nucleus to the hyphal tip) that organelles with a typical diffusivity ($D \approx 0.02\mu\text{m}^2/\text{s}$(14)) would require many hours to spread through the hypha by diffusion alone. Processive transport mechanisms such as hitchhiking are thus crucial to maintaining these organelles broadly distributed throughout the cell.

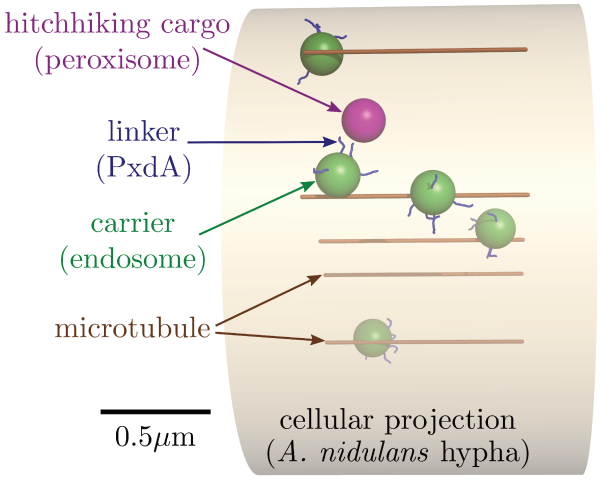

Figure 1: Schematic of the model for hitch-hiking initiation. A simulation snapshot is shown with all model components labeled. Specific components for peroxisome hitchhiking in *Aspergillus nidulans* are indicated in parentheses. Scale bar: 0.5μm.

In this paper we investigate the effects of cellular and cytoskeletal geometry, as well as mechanical properties of the transport machinery, on the initiation of hitchhiking runs by a cargo that encounters and attaches to a carrier organelle. We develop an analytical and computational model of hitchhiking transport initiation within tubular geometries, quantifying the rate of cargo-carrier contact for a wide range of biologically feasible parameters. In particular, we focus on peroxisome hitchhiking in fungal hyphae, leveraging experimental observations to identify the relevant parameter regime. We analyze the role of linker proteins in mediating the contact between carrier and cargo organelle, and establish optimum mechanical and structural parameters for linkers that can maximize the hitchhiking initiation rate. For organelles that can tether to microtubule tracks, we quantify the potential enhancement of the hitchhiking rate due to tethering, and identify its effect on overall organelle dispersion in the cell.

METHODS

Overdamped Brownian dynamics simulations are employed to explore the dynamics of carrier and cargo organelles as they first encounter each other for hitchhiking initiation. Our focus is on the parameter regime where the following conditions are applicable: 1) a cylindrical domain with parallel microtubule tracks, 2) carrier and cargo organelles that are substantially smaller than the domain width, 3) cargo organelles that are sufficiently sparse to preclude cargo-cargo interactions, 4) linker proteins of length smaller than the domain width. In particular, these conditions are relevant to the dynamics of hitchhiking peroxisomes, carried by early endosomes in fungal hyphae.

The carriers (*e.g.*: endosomes) are modeled as spheres of radius $r_e = 100$nm, moving in a domain of length $L = 1\mu$m and radius $R = 1\mu$m with periodic boundaries in the axial direction. The radius of the domain is set to match the typical radius of fungal hyphae (see Supplemental Materials for measurements in *A. nidulans*)(14). The domain represents a section of cell around a single cargo capable of hitchhiking. In *A. nidulans* hyphae, peroxisomes are observed at an average linear density of approximately 1 organelle within a 1μm long region of the hypha (see Supplemental Materials), which sets the length of our simulated domain. This length allows us to assume only one peroxisome within the domain of interest, neglecting second-order effects. It should be noted that the fraction of peroxisomes actually engaged in hitchhiking at any given time is quite small (approximately 5% in *U. maydis* hyphae(14)). Given a density of linker-bearing endosomes of approximately 3 per μm (see Supplemental Materials), we would expect less than 2% of carrier organelles to be already encumbered by a hitchhiker. We therefore assume all carriers that enter the domain are not carrying a hitchhiker. For simplicity, our model also ignores any carrier organelles not capable of initiating hitchhiking (*eg:* due to lack of linkers) and any other organelles in the cell that do not serve as carriers. These additional components could provide buffeting effects through sterics or hydrodynamic entrainment(31) which are not included in our model.

Microtubules are modeled as N straight lines distributed uniformly within the domain cross section. Microtubule dynamics are not included in the current model, although they provide an interesting avenue for future study. We ignore transverse fluctuations of microtubules, given that their persistence length *in vivo* ($l_p \approx 30\mu$m (32)) is much longer than the domain length. The linear density of carrier organelles (ρ) gives the number of carriers per unit length of hypha. Our simulation includes ρL carriers within the simulated domain. Each carrier is attached to a microtubule track by a single zero-length stiff spring representing a molecular motor complex. The attachment point of the spring to the microtubule moves processively in either direction at a constant velocity of 2μm/s, comparable to the measured velocities of fungal peroxisomes and early endosomes(13). Upon leaving the domain, the carrier organelle reappears at the other side, on a newly selected microtubule, thereby maintaining a constant carrier density while representing organelles whose typical run-length is much longer than the domain length L.

Cargo organelles (*e.g.:* peroxisomes) are represented by spheres of radius $r_p = 100$nm, which either diffuse freely through the domain, or have a point on their surface attached to a fixed microtubule at the axial center of the domain. Both carriers and cargo experience Brownian forces and torques corresponding to translational diffusivity $D_t = k_bT/(6\pi\eta r)$ and rotational diffusivity $D_r = k_bT/(8\pi\eta r^3)$, where η is the viscosity of the domain. The viscosity is chosen such that $D_t \approx 0.014\mu\text{m}^2/\text{s}$ for the cargo organelle, in keeping with measured diffusivities of peroxisomes in *Ustilago maydis* hyphae(14). Steric interactions between organelles and with the cylindrical boundary of the domain are implemented using a stiff harmonic potential.

The simulations are evolved forward using a fourth-order Runge-Kutta algorithm(33) with time-steps of 10^{-4}s. Each simulation trial is run for a total of 5s, allowing each carrier to pass 10 times through the domain. 2500 trials are carried out for each combination of carrier density ρ and microtubule number N.

Linker proteins that mediate contact between carrier and cargo are modeled as continuous semiflexible worm-like chain (WLC) polymers (34) with varying length. Positions of the base of the linker protein are chosen uniformly on the carrier surface, and the initial linker tangent is assumed perpendicular to the surface. Using analytically calculated distributions for the end point of a WLC(35), we tabulate the spatial distribution of the probability that a cargo organelle overlaps with the tip of a linker for a given configuration of the carrier and cargo (see Supplemental Materials). Using this tabulated probability, at each time step we check whether linker-mediated contact between the carrier and cargo has occurred. This approach avoids resolving the dynamics of the linker protein configurations, working instead in the fast-equilibration limit where the position of each linker tip is sampled from its equilibrium distribution at each timestep.

For each simulation trial, we record the time until the single cargo organelle first contacts either the carrier surface or the tip of a linker protein. We note that these encounter times provide a lower limit on the waiting time until hitchhiking initiation. Namely, in Fig. 2-5 we assume that each encounter successfully and immediately results in a hitchhiking event. The role of unsuccessful encounters is explored in a subsequent section (Fig. 7) by introducing a finite reaction rate k_{rxn} for initiating a successful hitchhiking interaction while the linker and cargo are in contact.

The empirical cumulative distribution function for contact events is used to extract an effective rate of contact. Over the simulation timescale, the cumulative distribution functions observed fit well to a double exponential form $Q(t) = 1 - f_1 e^{-t/\tau_1} - f_2 e^{-t/\tau_2}$ (see Supplemental Materials). This functional form is chosen *ad hoc* to enable smooth interpo-

lation of the data within the simulation time-frame, and extrapolation to longer times, in order to calculate the average waiting time until contact. No specific physical meaning is assigned to the resulting two time scales. The average rate of hitchhiking initiation is defined by $k_{\text{hit}} = (f_1\tau_1 + f_2\tau_2)^{-1}$. Variation in this initiation rate is approximated by bootstrapping(36) over all simulation trials for a given set of parameters. All error bars shown give the standard error in k_{hit} over 100 bootstrapping runs.

Brownian dynamics simulation code (in Fortran90) and scripts for implementing linker distributions and obtaining encounter rates from simulation results are provided in a GitHub repository: https://github.com/lenafabr/hitchhiking_initiation.

RESULTS AND DISCUSSION

Rate of encounter with carrier organelles

The efficiency of hitchhiking transport initiation is governed in part by geometric parameters, such as the density of microtubules and carrier organelles, as well as the length and distribution of linkers on the carrier surface. In order to be picked up for a hitchhiking run, the cargo must be sufficiently close to a passing carrier to be able to engage with a linker protein. We begin first by considering the rate of encounters between a diffusing cargo organelle and a processively moving carrier. This rate corresponds to hitchhiking initiation in the limit of very short, densely packed linkers, where the entire carrier surface is capable of binding the cargo.

A Brownian dynamics simulation framework is employed to explore how the density of microtubules and carriers modulates organelle encounter in a tubular region of radius $R = 1\mu$m with parameters relevant to peroxisome transport in hyphae (Fig. 1). The radius of the tubular region corresponds to the average radius of *A. nidulans* hyphae, as obtained from experimental measurements (see Supplemental Materials). A variable number (N) of parallel microtubules are uniformly scattered throughout the tubular region. A single cargo of radius $r_p = 100$nm and translational diffusivity $D_t = 0.014\mu\text{m}^2/\text{s}$ represents the peroxisome and a variable linear density ρ of carrier organelles of radius $r_e = 100$nm move with processive velocity $v = 2\mu$m/s along the microtubule tracks. Brownian forces on the carrier organelles drive fluctuations around their attachment point to the microtubules. Periodic axial boundary conditions allow for maintenance of a constant density of processively moving carriers in the local vicinity of the cargo.

In order to come in contact with a carrier, the cargo must first approach sufficiently close to a microtubule track (within a distance of $r_p + 2r_e = 0.3\mu$m), and then be hit by a passing carrier before moving away from the track again (Fig. 2a). For a single, centrally located microtubule, the region of proximity covers a fraction $f_1 = (r_p + 2r_e)^2/(R - r_p)^2 \approx 0.1$ of the available cross-sectional domain area. As multiple parallel microtubules are placed within the domain, their proximity regions cover an increasing fraction of the cross-sectional area. We vary the number of microtubules N in our simulation, randomizing the placement of each microtubule and the initial radial position of the peroxisome within the domain. Fig. 2b shows the fraction of iterations where the peroxisome starts within reach of a microtubule (equivalent to the MT-proximal area fraction f_N), as well as k_{MT}, an effective rate for peroxisomes initiated outside of the MT-proximal area to first reach this area (see Methods for details of rate calculations).

The time for a cargo to encounter a passing carrier is governed both by the dynamics of entering and leaving the MT-proximal region (rates k_{MT}, k_{leave}) and the rate k_{pass} of carrier passage in the vicinity of a cargo that is within reach of a microtubule. Because the velocity of processive motion is rapid compared to the cargo diffusivity, we treat the carrier arrival as a constant rate process while the peroxisome is within the MT-proximal region. The rate of this arrival is given by

$$k_{\text{pass}} = v\rho\frac{(r_e + r_p)^2}{f_N(R - r_p)^2}, \tag{1}$$

where $v\rho$ is the rate at which carriers pass the axial position of the cargo and the second term corresponds to the equilibrium probability that the radial position of the passing carrier is within reach of the cargo, assuming the cargo is uniformly distributed within the MT-proximal area. The effective rate of leaving the MT-proximal area must be such that the cargo spends fraction f_N of its time within this area at equilibrium. Namely, $k_{\text{leave}} = k_{\text{MT}}[1 - f_N]/f_N$. These three rates allow for an approximate calculation of the waiting time for a cargo organelle distributed uniformly within the domain to first encounter a carrier, using the simplified kinetic scheme shown in Fig. 2a. The inverse of this time gives the effective carrier encounter rate (see Supplemental Material for derivation):

$$k_{\text{carrier}} = \frac{k_{\text{pass}}k_{\text{MT}}(k_{\text{leave}} + k_{\text{MT}})}{k_{\text{pass}}k_{\text{leave}} + (k_{\text{MT}} + k_{\text{leave}})^2}. \tag{2}$$

When carrier passage is very frequent ($k_{\text{pass}} \to \infty$), the average time to carrier encounter reduces to $1/k_{\text{carrier}} \to (1 - f_N)(1/k_{\text{MT}})$, equivalent to the probability the cargo starts outside of the microtubule region multiplied by the time to reach that region.

The typical time-scale for cargo-carrier encounter in simulated trajectories is obtained by fitting the computed cumulative distribution function to a double exponential process (Fig. 2c; details in Supplemental Material). As shown in Fig. 2d, effective encounter rates obtained from the simulations are well represented by the simplified kinetic model of Eq. 2.

At low carrier density, increasing the microtubule number beyond a couple of microtubules has little effect on the rate with which the cargo first encounters a carrier. In this

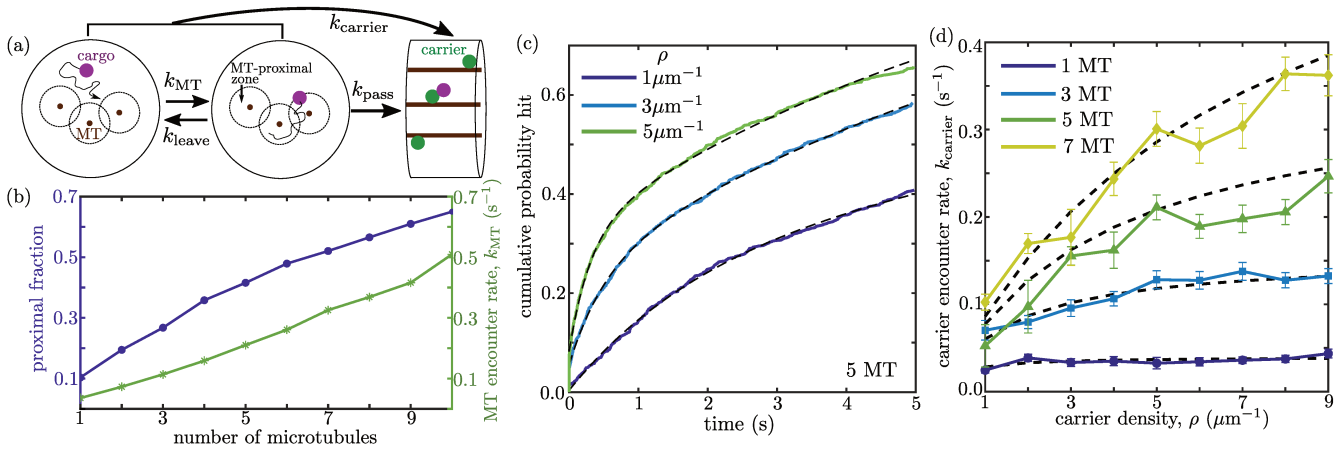

Figure 2: Dynamics of cargo encounter with carrier organelles. (a) Schematic model for carrier encounter, illustrating the two-step process of first entering a MT-proximal zone, then waiting for a carrier passage event. (b) Average fraction of domain cross-sectional area within distance $2r_e + r_p$ from a microtubule (left) and rate k_{MT} to encounter a microtubule if starting outside the proximal zone (right). (c) Cumulative distribution of carrier encounter times, plotted for simulations with three different carrier densities. Dashed lines give fit to a double-exponential function used to extract an effective encounter rate. (d) Average carrier encounter rate, for different numbers of microtubules and carrier density. Symbols indicate simulation results; dashed black lines show predictions from approximate kinetic model (Eq. 2).

regime, the diffusing cargo has time to enter and leave the MT-proximal region while waiting for a carrier to pass by. Each carrier passage event becomes essentially independent from the previous one, in terms of the probability that it will hit the cargo. Splitting up a fixed carrier density across more microtubules does not change the overall frequency of these independent passage events and thus has little effect on the encounter rate. By contrast, at higher carrier densities increasing the number of parallel microtubules can greatly speed up the encounter process. In this limit, carriers arrive very rapidly and the encounter is limited by the cargo approaching sufficiently close to a microtubule to enable contact. Hence, increasing k_{MT} by raising the number of microtubules will increase the overall encounter rate.

Similarly, when there are very few microtubules in the domain, the encounter rate is nearly independent of the carrier density. A greater frequency of carrier passage events along a single microtubule will not speed up encounter times that are dominated by the cargo coming in radial proximity of that microtubule. At higher microtubule numbers, the cargo spends most of its time within the MT-proximal region and increasing carrier density enhances the rate at which some carrier passes the cargo on a nearby microtubule.

We quantified the number of microtubule plus-ends in *Aspergillus nidulans* hyphae, and found approximately $N \approx 5$ parallel microtubules at the hyphal tips (see Supplemental Materials). For this number of microtubules, the rate of cargo encounter with a carrier increases with the carrier linear density up to $\rho \approx 5\mu\mathrm{m}^{-1}$, after which it is insensitive to the presence of additional carrier organelles. We also quantified the linear density of fluorescently-tagged early endosomes in *A. nidulans* hyphae and found approximately 5 endosomes per μm length of hypha (see Supplemental Materials). As approximately 55% of endosomes carry the PxdA linker protein responsible for peroxisome hitchhiking(13), we would expect the rate of peroxisome encounter with a PxdA-bearing endosome ($\rho \approx 2.8\mu\mathrm{m}^{-1}$) to be approximately $0.2\mathrm{s}^{-1}$.

Rate of encounter with linker proteins

Organelle hitchhiking is generally believed to involve the cargo (hitchhiker) attaching to a carrier organelle surface via one or more linker proteins (16). For the case of peroxisome transport in *A. nidulans*, the putative linker protein (PxdA) is present on a subpopulation of early endosomes and is required for peroxisome hitchhiking (13). This protein contains a long predicted coiled-coil region, which is approximately 90nm in length if fully extended(13). Given that the linker protein may be comparable in size to the organelles themselves, its length, distribution, and mechanical properties have the potential to substantially impact the efficiency of hitchhiking initiation. We thus incorporate extended linker proteins on the carrier surface into our dynamic model and proceed to explore how linker protein parameters modulate the rate at which the cargo organelle can get picked up for a hitchhiking run.

We use a multi-scale approach to integrate the linkers into our Brownian dynamics simulations. The linkers are treated as semiflexible "worm-like" chains (WLC)(34) of length ℓ, with one end fixed at a given position on the endosome and the initial tangent fixed to be perpendicular to the endosome surface. It is not known whether linker proteins are capable of diffusing over the carrier surface. In the extreme case of very rapidly diffusing linkers, any close approach of the hitchhiking

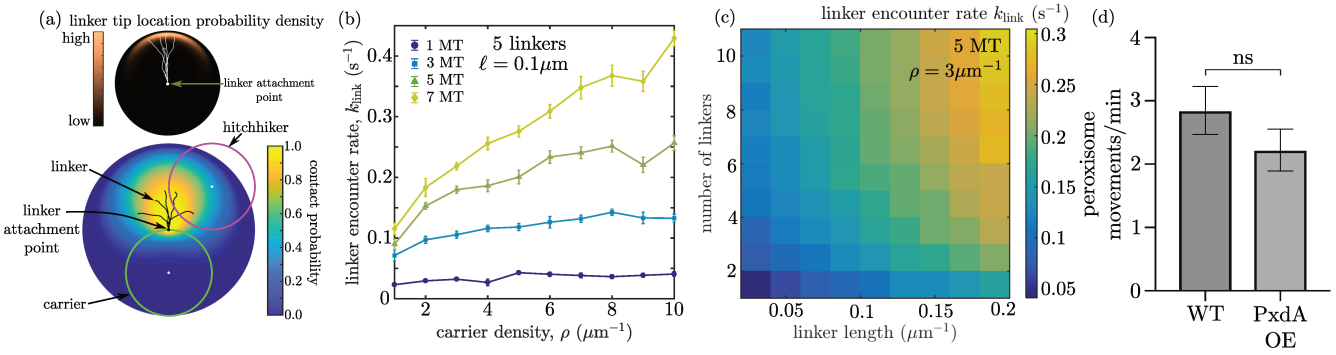

Figure 3: Rates of encounter with hitchhiking linkers. (a) Model of linker protein chains attached to carrier surface. Top: end distribution of a WLC of length $\ell = \ell_p$, with initial end orientation fixed. Representative configurations of the linker are indicated in white. The color represents the probability density of the linker tip location. Bottom: probability of contact between the tip of a linker (black lines) on a carrier (green) and the hitchhiking cargo (magenta). The color represents the contact probability for each position of the hitchiker center relative to the linker attachment point. (b) Rate at which the cargo encounters the first linker tip, as a function of the carrier density and the number of microtubules. (c) Effect of linker length and linker number per carrier on the encounter rate. (d) Bar graph of the peroxisome flux in wild-type (WT) hyphae and hyphae overexpressing PxdA(Δ1-500)-TagGFP (PxdA OE). Peroxisome flux is quantified as the number of peroxisome movements across a line drawn 10μm from the hyphal tip in a 1 minute movie. Wild-type hyphae had 2.84 ± 0.38 (SEM) peroxisome movements per minute, while hyphae with overexpressed PxdA(Δ1-500)-TagGFP had 2.22 ± 0.33 (SEM) peroxisome movements per minute. $p = 0.2569$, Mann-Whitney test. Error bars=SEM. $n = 46$ WT hyphae and 49 PxdA OE hyphae. See Supplementary Material for details of peroxisome flux quantification.

cargo to the moving carrier would result in an encounter with a linker, given that the proteins could explore the entire carrier surface very fast compared to the relative motion of the organelles. This limiting case approaches the situation where the entire carrier surface is capable of interacting with the cargo, as discussed in the previous section, albeit with an expanded effective carrier radius resulting from the added extension of the linker beyond the carrier surface. We focus here on the opposite limit, where a given number of linker proteins is attached to fixed points on the carrier surface with no diffusion permitted for the attachment points.

Assuming that the conformation of an individual linker protein equilibrates much faster than the large organelle movements, we employ a separation of timescales in our simulation. Specifically, we assume that each linker samples its configuration from an equilibrium distribution independently on each Brownian dynamics step. We make use of the analytically known distribution function for a WLC with fixed end orientation (35) to compute the probability that a free linker end will intersect with the hitchhiking cargo for a given position of the cargo relative to the anchoring point of the linker (Fig. 3a). These probability distributions are used to sample whether the cargo has come into contact with a linker tip during each simulation step. The hitchhiking initiation time is then taken to be the total simulation time until the first such contact with a linker tip occurs. We note that this model assumes all contacts between a linker tip and a cargo organelle lead to rapid formation of a long-lasting interaction that results in a hitchhiking run. In particular, the entire surface of the hitchhiking cargo is assumed capable of interacting with the linker protein. The hitchhiking rates discussed here are thus an upper estimate on actual initiation rates.

The rate of encounter with a linker tip shows a similar dependence on microtubule and carrier density (Fig. 3b) as the rate of coming into contact with the carrier organelle itself (Fig. 2b), discussed in the previous section. Specifically, increasing the carrier density has little effect for low microtubule numbers. Interestingly, the rates of linker contact are quite similar to the rate of carrier contact, even for a fairly small number of linkers on the carrier surface. Fig. 3c shows how the rate of linker encounter with cargo depends on the number and length of the linkers. Due to the flexibility and length of the linker proteins, only a small number of linkers (~ 5, for linkers of size comparable to the putative PxdA coiled-coil region) is sufficient to obtain near maximum initiation rates. This prediction from the physical model is consistent with experimental measurements, which show that overexpressing PxdA linker proteins in *A. nidulans* does not increase the rate of hitchhiking initiation (Fig. 3d, Supplemental Videos S1, S2).

Using the standard expansion for a nearly straight worm-like chain, the linker tip will project a typical distance $\Delta z \approx \ell[1 - \ell/(6\ell_p)]$ from the carrier surface(37). For proteins of length $\ell = 100$nm and persistence length $\ell_p = 100$nm, a single instantaneous encounter between cargo and carrier surface is expected to yield a roughly 6% chance of any

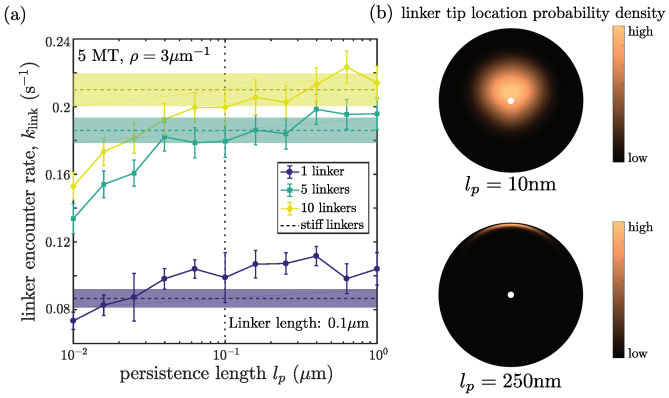

Figure 4: Dependence of encounter rate on linker flexibility. (a) Rate at which cargo encounters a linker tip, as a function of linker persistence length for different linker numbers. Dashed lines with shaded areas denote contact rate for infinitely stiff linkers along with standard error. Dotted vertical line denotes $l_p = 0.1\mu$m, used in all other simulations. (b) End distribution of a WLC of length $\ell = 100nm$ with initial orientation fixed, highlighting the increased extension Δz yet smaller area coverage of stiffer linkers. Top: l_p = 10nm, bottom: l_p = 250nm

given linker on that carrier intersecting with the cargo. For 5 independent linkers, this means that approximately 30% of carrier encounters will result in immediate linker contact. This fraction is increased further because the diffusion of cargo and carrier during a passage event allows them to sample a greater fraction of each other's surface, as has been quantified for the case of molecular diffusion towards receptor patches on a sphere(38).

In addition, by projecting beyond the surface of the carrier, the linker proteins serve as antennae, allowing contact while the cargo is further away from the carrier. This type of interaction effectively replaces r_e with $r_e + \Delta z$ and results in more rapid encounters. Consequently, for long and numerous linkers, the rate of initiation can be even faster than the rate of contact with the carrier. This effect arises from the extra range afforded by long linker proteins, allowing contact with the linker to occur while the cargo is still at a substantial distance from the carrier surface.

The rate at which linker contact occurs depends not only on the geometry and density of the linker proteins, but also on their flexibility (Fig. 4). In order to project beyond the surface of the carrier organelle, the linker proteins must be relatively stiff ($\ell_p \gtrsim \ell$). For linkers with a substantially shorter persistence length, the smaller value of Δz implies that the cargo organelle would need to approach closer to the carrier surface in order to have a high likelihood of encountering the linker tip (Fig. 4b). Interestingly, when there is only one linker on each carrier, a slight optimum in linker flexibility is observed. This effect arises from the fact that the tip of a stiffer linker thermally explores a smaller area in the plane parallel to the surface of the carrier. Thus, when linker density is low, semiflexible linkers with ℓ_p comparable to ℓ increase the probability of an encounter with the linker tip each time the cargo approaches a carrier, above what it would be for infinitely stiff linkers. We note that the effective persistence length of coiled-coil protein structures is reported to be in the range of 30 – 170nm (39–42). While the detailed structure and mechanical properties of the PxdA linker are unknown, this protein appears to fall in the expected range for an efficient hitchhiking linker – namely, it has a predicted coiled-coil domain with comparable persistence length and end-to-end length. The coiled-coil domain of PxdA is thus expected to have sufficient stiffness that would allow the protein to project beyond the endosome surface, while remaining sufficiently flexible so that the linker tip could explore a substantial area around its attachment point.

Tethering to microtubules enhances the rate of hitchhiking initiation

A number of organelles, including mitochondria, melanophores, and peroxisomes are known to become tethered to microtubule tracks by regulatory proteins that are crucial for maintaining their cellular distribution(23, 25, 28, 43, 44). Such tethering not only helps localize organelles along extended cell regions (as in neurons) (27, 43) but is also thought to facilitate interactions between multiple organelles by restricting their three-dimensional diffusion through the cytoplasm(28). In the case of hitchhiking cargos such as peroxisomes in *Aspergillus* and *Ustilago*, tethering to a microtubule has the potential to enhance the rate of hitchhiking initiation by eliminating the time spent out of reach of the microtubule-bound carrier organelles. We explore the effect of cargo tethering in the context of our hitchhiking initiation model by attaching the cargo surface to a randomly selected microtubule and quantifying the rate at which the cargo first encounters the carrier surface or a carrier-borne linker protein.

Tethering of the cargo to a microtubule substantially increases the rate of encounter with a carrier organelle, particularly in the case of low microtubule density (Fig. 5a). This enhancement arises from two related effects. First, the lower volume available to the cargo makes it much more likely in equilibrium (and hence at the start of the simulation) that the cargo starts in close contact with a carrier organelle. This is particularly the case for high carrier densities and low microtubule numbers, where the carriers cover nearly the entire volume available to tethered cargo. A related effect is that, even for cargos that start far from any carrier, the need to first reach a microtubule track is eliminated ($k_{MT} \to \infty$), so that the rate of carrier encounter becomes comparable with the rate of carriers passing a hyphal cross-section along the same (or nearby) microtubule.

When the hitchhiking cargo is tethered to a microtubule, increasing the number of microtubules along the hypha greatly slows the rate of encounter with a passing carrier. Because

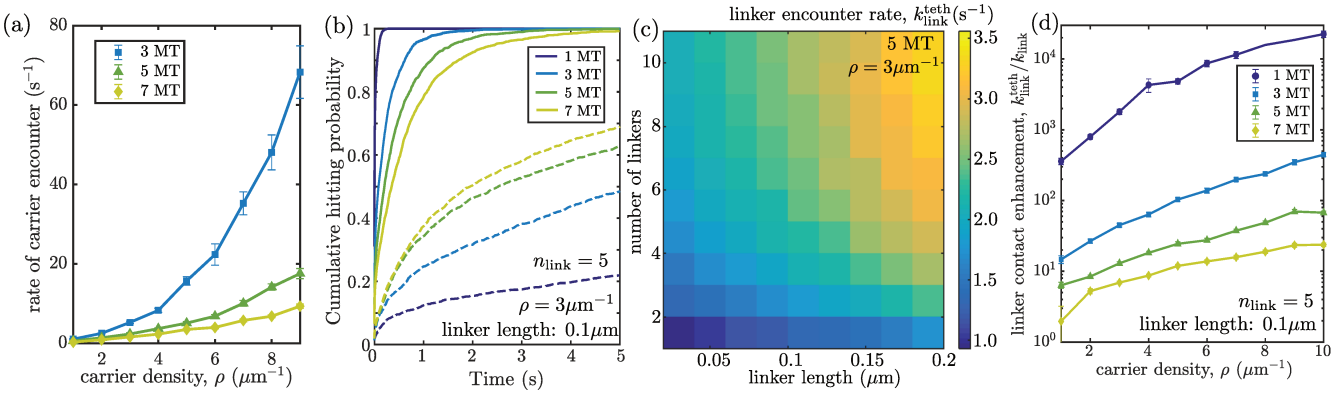

Figure 5: Effect of cargo tethering to microtubule on encounter rates with carrier organelles and their linker proteins. (a) Rate of encounter with a carrier organelle, for different numbers of microtubules in the domain. (b) Cumulative hitting probability with the tip of a linker protein, for tethered (solid lines) and untethered cargo (dashed lines), showing more rapid encounters in the tethered case. (c) Enhancement of overall contact rate with a linker protein tip, due to tethering of cargo. (d) Encounter rate between a tethered cargo and linker protein tip, as a function of linker length and number. (e) Ratio of encounter rates with linker protein tips, for a tethered versus diffusive cargo.

we assume a constant linear density of carrier organelles per length of hypha, additional microtubules provide more options for where the carriers are located in the hyphal cross-section, diverting some of them away from the one microtubule to which the cargo organelle is attached. Hence, fewer microtubules makes it more likely that each carrier will come in contact with the cargo as it passes the relevant cross-section of the hypha.

When hitchhiking initiation requires encounter with the tip of a linker protein, tethering of the cargo can also greatly increase the rate at which such encounters occur (Fig. 5b-d). Unsurprisingly, tethering has the greatest effect on encounter rates at low microtubule numbers and short linker lengths, where facilitating the rate at which the cargo comes near the carrier surface has a large effect on the hitchhiking initiation. For high microtubule numbers and long linkers, the effect of tethering is less pronounced because even freely diffusing cargos spend most of their time within the maximum distance ($r_p + 2r_e + \Delta z$) of the microtubule tracks that allows for hitchhiking initiation during carrier passage events. As seen in Fig. 5d, tethering plays a greater role when the carrier density is high, since it is in this regime where contact with diffusive cargo is rate-limited by the cargo coming in proximity of a microtubule track. At lower carrier densities, the encounter time is dominated by waiting for a carrier passage event and tethering to a microtubule has less effect.

For the typical microtubule and PxdA bearing early endosome density observed in *A. nidulans* hyphae ($N \approx 5$, $\rho \approx 3\mu m^{-1}$; see Supplemental Materials), and for the predicted PxdA coiled-coil linker length ($\ell \approx 90$nm), tethering of peroxisomes is expected to increase the rate of hitchhiking initiation by more than 12-fold (Fig. 5d). Peroxisome hitchhiking in hyphae can thus be greatly enhanced by attaching the peroxisomes to microtubules. The enhancement remains substantial even if the peroxisomes are assumed to be much larger (8-fold enhancement for $r_p = 300$nm; see Supplemental Material). Published kymographs of labeled peroxisomes in $\Delta pxdA$ hyphae(13) hint that peroxisomes exhibit little axial motion over time periods of up to 10 sec. While time-sampling limitations of this data preclude a definitive demonstration of tethering, the observed motion is not inconsistent with these organelles being attached to stationary cellular structures. Furthermore, in human cells, the peroxisomal membrane protein PEX14 has been shown to bind to tubulin and to be critical for peroxisome motility along microtubules(23). There is thus reason to propose that fungal peroxisomes may also be attached to microtubules and, as shown here, that this tethering may contribute to their ability to hitchhike throughout the hypha.

Success rate for hitchhiking initiation

Our mechanical model indicates that, for parameters relevant to *A. nidulans* hyphae, the rate at which a peroxisome encounters a PxdA linker on a passing endosome is approximately $0.2s^{-1}$ if the peroxisome is untethered and approximately $2s^{-1}$ if it is tethered to a microtubule. These timescales set an upper limit to the rate of hitchhiking initiation, since not all encounters with the linker will result in a successful hitchhiking run.

We can measure the initiation rate for peroxisome hitchhiking directly by tracking individual peroxisome trajectories obtained from time-lapse Lattice light sheet imaging of *A. nidulans* hyphae. A wavelet-based adaptive thresholding algorithm(45) is leveraged to classify sections of the particle trajectories as processive runs versus passive motion (Fig. 6a; see Supplemental Materials). For all trajectories with an ac-

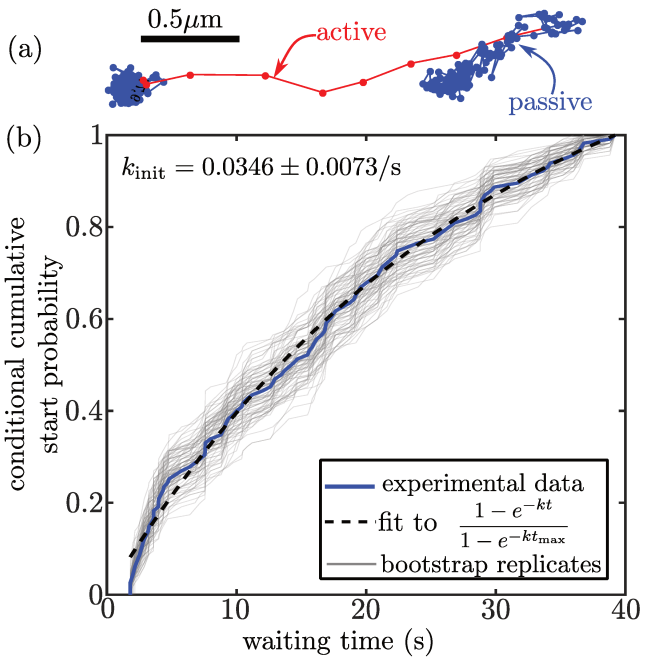

Figure 6: Experimentally measured hitchhiking initiation rate for peroxisomes in *A. nidulans* hyphae. (a) Example trajectory of individual peroxisomes, with passive segments marked in blue and active segments in red. (b) Cumulative distribution of start times for active motion, conditional on an active run occuring during the measured time window ($t_{\max}$). Grey curves show variation from bootstrapping. Dashed line gives fit to conditional cumulative distribution of Poisson process.

tive run of duration at least 1sec, we look at the distributions of times from the start of the trajectory until the active run is initiated (Fig. 6b). The empirical cumulative distribution function is fitted to the conditional cumulative distribution for a Poisson process with a constant rate k_{init}, given that an event occurs before the end of the tracking period ($t_{\max}$). The resulting estimate for the hitchhiking initiation rate is $k_{\text{init}} = 0.035 \pm 0.007\text{s}^{-1}$. This rate of hitchhiking initiation is nearly an order of magnitude lower than our predicted rate of linker protein encounter, even for untethered peroxisomes.

This discrepancy implies that only a small fraction of encounter events with the PxdA linkers result in the successful initiation of a hitchhiking run. We therefore incorporate unsuccessful encounters directly into our model by introducing another rate constant k_{rxn}, giving the rate at which a successful binding reaction occurs between the linker protein and the peroxisome surface, while the two are within contact distance of each other. This is a microscopic rate constant effectively incorporating the molecular-scale sampling of the peroxisome surface by the linker, after it has already come within binding range. The higher the value of k_{rxn}, the more likely a linker encounter of a certain duration will result in the successful initiation of hitchhiking. The base model described in previous sections corresponds to the limit with $k_{\text{rxn}} \to \infty$, when all encounters result in a hitchhiking run. As k_{rxn} decreases, many encounters are unsuccessful and the expected rate of hitchhiking initiation diminishes dramatically (Fig. 7a).

In addition to finding the time until first encounter, the simulations can also be used to quantify the distribution of durations for each linker encounter event ($P_{\text{enc}}(t)$; see Supplemental Material). The average duration for a diffusive peroxisome encounter with a linker protein is found to be $\overline{\tau}_{\text{enc}}^{\text{diff}} \approx 0.03\text{s}$, whereas the average duration for a tethered peroxisome encounter is $\overline{\tau}_{\text{enc}}^{\text{teth}} = 0.1\text{s}$ (Fig. 7b). Tethered peroxisomes tend to experience longer encounters with a linker, as the carrier organelle passes by and maneuvers around the cargo on the microtubule. Using the distribution of encounter durations, we can find the average probability that a linker encounter event will be successful for a given k_{rxn}. This relationship is given by

$$p_{\text{success}} = 1 - \int_0^\infty P_{\text{enc}}(t) e^{-k_{\text{rxn}} t}\, dt. \tag{3}$$

Due to the longer duration of encounter events, the overall probability that an encounter will result in successful initiation is always higher for a tethered than a diffusive cargo (Fig. 7c). Interestingly, the ratio of hitchhiking initiation rates for tethered versus diffusive peroxisomes is largely insensitive to k_{rxn}, for values above $k_{\text{rxn}} \gtrsim 5\text{s}^{-1}$ (Fig. 7d), even though tethered encounters are up to 3-fold more likely to be successful. This observation indicates that individual encounters for diffusive peroxisomes are not independent of each other, so that even a short encounter with a linker protein means the peroxisome is in a position where subsequent encounters will happen frequently.

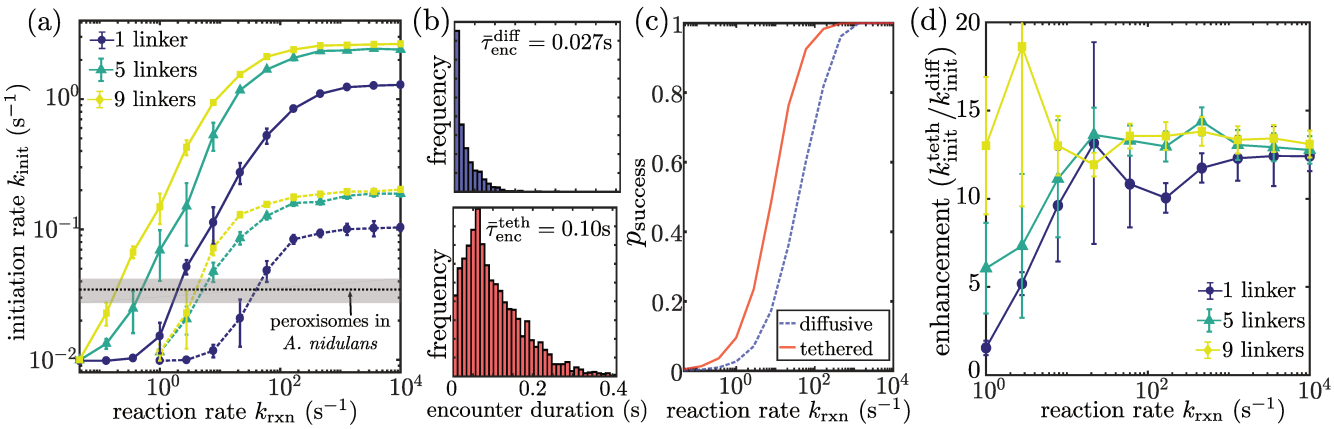

Figure 7: Hitchhiking initiation depends on rate of successful reaction between linker and cargo during an encounter event. (a) Overall rate of hitchhiking initiation, as a function of the reaction rate k_{rxn} for each linker. Dashed curves give results for diffusive cargo and solid curves for tethered cargo. Horizontal line represents experimentally measured initiation rate, with shaded region indicating standard error. (b) Distribution of encounter durations with an individual linker for diffusive (top) and tethered (bottom) cargo. (c) Probability of an encounter successfully resolving in hitchhiking for diffusive (dashed line) and tethered (solid line) cargo. (d) Enhancement in initiation rate due to tethering, for different values of k_{rxn}.

Comparison with the experimentally measured hitchhiking initiation rate (horizontal line in Fig. 7a) indicates that for untethered peroxisomes and a saturating number of linkers, the reaction rate is expected to be roughly $k_{\text{rxn}} \approx 4\text{s}^{-1}$, with corresponding success probability $p_{\text{success}} \approx 0.1$. If the peroxisomes are tethered, the probability of each encounter successfully initiating a hitchhiking run would need to be $p_{\text{success}} \approx 0.02$ to yield the observed initiation rate.

Such a low success rate may arise from a variety of biological or mechanical reasons. First, it is possible that an individual peroxisome and PxdA-bearing endosome are incabable of forming a hitchhiking interaction during a given encounter. In particular, it is unclear if PxdA is the actual linker between peroxisomes and early endosomes, or if it is only one component of a hitchhiking apparatus. It is also unclear if the coiled-coil region of PxdA is consistently in a fully extended form or if it takes on multiple conformations that may make it less capable of readily interacting with hitchhiking cargo. Other proteins may also regulate PxdA activity or be involved in linking peroxisomes to early endosomes in other ways. For example, only a certain percentage of peroxisomes may display a binding receptor for PxdA, creating a smaller pool of peroxisomes competent to hitchhike.

Furthermore, even if the peroxisome and the PxdA linker are capable of binding, this binding reaction may be comparatively slow, so that many contacts do not result in successful hitchhiking initiation. For instance, binding receptors on the peroxisome may not cover the entire surface, forcing the linker protein tip to explore a portion of the peroxisome surface before actually binding. The linker may also need to sample many conformations before making a successful contact with a receptor. As the proteins comprising the hitchhiking apparatus are unknown, the strengths of contacts between the peroxisome and early endosome are unclear and may be weak, resulting in broken contacts before hitchhiking is initiated. Finally, if peroxisomes are indeed tethered to microtubules, there may be a high energy requirement to break those tethers and initiate a hitchhiking event, resulting in an effectively slow reaction rate and a high fraction of unsuccessful encounters.

Given all of these potential effects beyond the encounter of a hitchhiking cargo with a linker protein, it is perhaps not surprising that such encounters should be much more frequent than actual hitchhiking initiation events. The geometric and mechanical parameters described here thus determine the frequency of opportunities for hitchhiking to occur. This sets an upper limit on the rate of hitchhiking initiation, for the case of easily broken tethers, a fully reactive peroxisome surface, and very rapid binding of the linker to the peroxisome surface.

Effect of initiation rate on overall cargo dispersion

Our exploration of the dynamics of cargo and carrier encounters indicates that tethering of cargo to microtubules can greatly enhance the rate of hitchhiking initiation. However, tethering of the cargo also inhibits its ability to move diffusively throughout the domain. Therefore, we sought to determine how these two competing factors (hindered diffusion but increased hitchhiking rate due to tethering of a cargo) would balance each other to affect the long-range dispersal of hitchhiking cargo organelles throughout a cylindrical region.

To address this, we switch to a simplified, analytically tractable model which focuses on the motion of hitchhiking cargo organelles along the hyphal axis. Specifically, we leverage the one-dimensional "halting creeper" model(19) where cargo organelles are treated as point particles subject

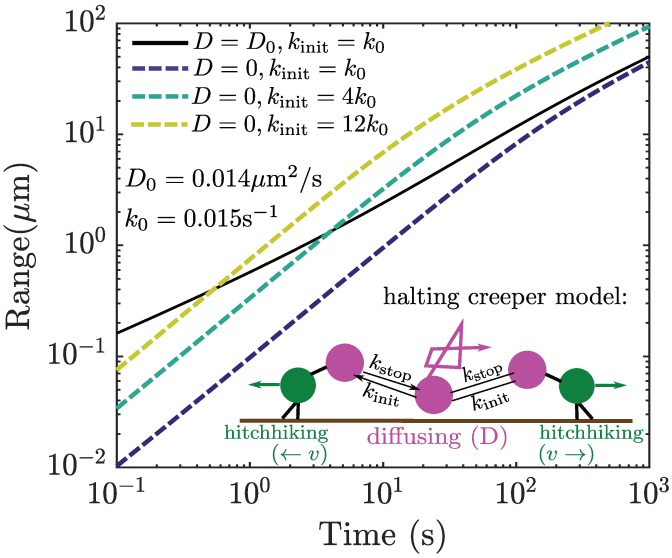

Figure 8: Range of a halting creeper particle engaged in bidirectional runs alternating with diffusive or tethered periods. Solid black line gives range for a particle that diffuses freely with diffusivity D_0, between processive runs initiated with a rate k_0. Dashed lines give range for particles that are tethered when not engaged in an active run, but with increasing initiation rates.

to multimodal transport. The particles exhibit memoryless stochastic switching between bidirectional processive motions (with velocity v, starting rate k_{init}, and stopping rate k_{stop}), interspersed with diffusive periods of diffusivity D (Fig. 8 inset). The more detailed mechanical model for hitchhiking initiation described in previous sections allows us to calculate the effective starting rate k_{init} with and without tethering of the cargo organelles to microtubules.

In prior work(19), we developed an analytical expression for the range of an exploring "halting creeper" particle. Particle range constitutes a metric of interest for intracellular transport processes because it enables direct calculation of the average time for any target in the cell to be found by the first of a uniformly distributed set of particles. It also provides an estimate for the distance from its site of biogenesis which an organelle explores over a finite time period. The range thus determines the extent to which organelles accumulate at their site of formation versus dispersing throughout the cell. It can be shown(19) that the range of a halting creeper transitions between a ballistic regime [range $Z(t) = fvt$] and an effectively diffusive regime [$Z(t) = \sqrt{4D_{\text{eff}}t/\pi}$], where $D_{\text{eff}} = (1-f)D + fv^2/k_{\text{stop}}$ is an effective long-time diffusivity, and $f = k_{\text{init}}/(k_{\text{init}} + k_{\text{stop}})$ is the equilibrium fraction of time in processive motion. The transition to the long-range diffusive regime occurs at a time $t^{**} = 16D_{\text{eff}}/(\pi f^2 v^2)$. Increasing the starting rate for processive motion (k_{init}) enhances the overall particle range at long times (above t^{**}), while decreasing the transition time where the effectively diffusive motion sets in. By contrast, in the absence of tethering, short-time motion is enhanced, creating a separate regime dominated by diffusion only with range $Z(t) = \sqrt{4Dt/\pi}$.

In Fig. 8 we show the expected range of particles with different combinations of diffusivity and processive starting rate. The solid line represents approximate parameters relevant to the motion of peroxisomes as measured in *Ustilago maydis* fungal hyphae, where the peroxisomes appear to exhibit diffusive, untethered motion between processive runs(14). Namely, we set diffusivity $D_0 = 0.014\mu\text{m}^2/\text{s}$, hitch-hiking velocity $v = 1.9\mu\text{m/s}$, and run-length $vk_{\text{stop}} = 6.5\mu\text{m}$. The initiation rate for processive runs is estimated at $k_0 = 0.015\text{s}^{-1}$, such that approximately 5% of peroxisomes are expected to be hitchhiking at any given time(14). Tethering of such particles to a microtubule will reduce the diffusivity to zero, but can enhance the starting rate by a factor of roughly 12-fold, for the case of 5 parallel microtubules (see Fig. 5d). We thus plot how such increased processive starting rate due to tethering can enhance the range of spreading particles over time. We note that even a 4-fold increase in the starting rate raises the range of the particles above a time-scale of a couple of seconds. The 12-fold increase estimated from our hitch-hiking simulations is expected to raise overall long-time particle range by a factor of about 3-fold.

The halting creeper model thus provides insight into the relation between organelle dispersion, the rate of hitchhiking initiation, and its enhancement due to tethering. It also highlights the possible consequences of a breakdown of the tethering mechanism leading to inefficient dispersion of organelles.

CONCLUSIONS

In this work, we describe a computational framework for elucidating the key physical parameters that govern the efficiency of hitchhiking initiation. Using an analytical approach, we delineate the effects of geometry and transport machinery on the rate of encounter between a carrier and a hitchhiking organelle. In particular, we focus on the effects of the number of cytoskeletal tracks upon which the carrier organelles move and the linear density of the carriers. We show that encounter rates are nearly independent of the carrier density for low microtubule numbers, where the process is dominated by the ability of the diffusing cargo to come within proximity of a microtubule track. Splitting up the same carrier density across larger number of microtubules can improve the encounter rate through increasing the cross-sectional coverage by the moving carriers.

In some cells, linker proteins are known to mediate the contact between a carrier and a hitchhiking organelle. We calculate the rate of encounter between a carrier and a hitchhiking organelle as a function of the length and the number of linkers on the carrier. Our results show that very few linkers of moderate length are sufficient to saturate the contact rate. This result helps explain experimental measurements showing that

overexpression of PxdA linker protein does not increase the hitchhiking frequency of peroxisomes in *A. nidulans* fungal hyphae. Further exploring the effects of linker flexibility, we show that moderately stiff linkers provide optimal contact rates between the carrier and hitchhiking cargo, by allowing the linker tips to explore large volumes of space while extending substantially above the surface of the carrier.

Leveraging our simulation framework, we study the effect of tethering organelles to microtubules on the initiation of hitchhiking. The increased proximity to moving carriers results in a large enhancement of the contact rate, an effect that is particularly pronounced for small microtubule numbers and high carrier densities. Comparison of computed rates for cargo-linker encounter and and measured hitchhiking initiation rates for peroxisomes in *A. nidulans* hyphae indicates that only a small fraction of encounter events appear to result in successful hitchhiking. Nevertheless, by increasing the frequency of opportunities for such contact events to occur, tethering of the peroxisomes to microtubules is expected to enhance the rate of hitchhiking initiation by about an order of magnitude.

Based on this enhancement in the initiation rate, we compute the increased range covered by organelles exploring the cell through rare, sporadic hitchhiking runs. Our results show that tethering can substantially increase the amount of intracellular space explored over time-scales of seconds or higher, despite restricting diffusive transport.

Our computational framework is generally applicable to any transport process that relies on attaching to a carrier organelle, either directly or through stiff or flexible linker proteins. While we focus on the simple geometry of a cylindrical domain, the parameters employed here (carrier density, density of parallel microtubules) are local in nature. Hence, the initiation rates found can be applied to any system where microtubules are arranged in a parallel fashion around the current position of the cargo organelle. This includes cellular projections such as fungal hyphae and neuronal axons and dendrites, as well as micron-sized regions of the cell soma with no microtubule intersections. Hitchhiking initiation rates in the vicinity of intersecting microtubules are left as an extension of interest for further study.

Another topic of further interest is characterizing the biophysical processes that determine the duration and processivity of a hitchhiking run. In past studies where motor-driven organelles are observed to halt or change direction, such terminations of processive motion were attributed to microtubule intersections(22, 46, 47), tug-of-war between multiple motors(20), changes in motor activation state(48), or obstacles encountered by the organelle(47, 49) or the motors themselves(50). The effect of a hitchhiking cargo on all of these processes governing the run-length of a motor-driven carrier is currently unclear. Furthermore, additional mechanisms may be responsible for terminating or regulating hitchhiking runs specifically, including dissociation of the hitchhiker from the carrier and tug-of-war or cooperative events that may arise from a single cargo attaching to two different carriers. Establishing the underlying physical mechanisms that determine hitchhiking run-length is a fruitful topic for future study, necessary to developing a complete quantitative understanding of this non-canonical mode of intracellular transport.

AUTHOR CONTRIBUTIONS

SSM and EFK conceived and designed the research, and developed the model. SSM performed imaging studies, analyzed imaging data, and implemented simulations. JRC, CSN, and SLRP generated experimental data and performed imaging studies. All authors contributed to data interpretation and writing of the manuscript.

ACKNOWLEDGMENTS

We thank Hiroyuki Hakozaki for assistance with lattice light sheet imaging and processing as well as the Nikon Imaging Center at UC San Diego for help with imaging and data analysis.

SSM acknowledges funding via a predoctoral fellowship from the Visible Molecular Cell Consortium / Center for Transscale Structural Biology and Biophysics; EFK was supported by a fellowship from the Alfred P. Sloan Foundation and funding from the National Science Foundation CAREER Award Program (#1848057). JRC is funded by a postdoctoral fellowship from the National Institutes of Health (F32GM126692) and SLRP is funded by the Howard Hughes Medical Institute and the National Institutes of Health (R01GM121772).

SUPPLEMENTARY MATERIAL

An online supplement to this article can be found by visiting BJ Online at http://www.biophysj.org.

SUPPORTING CITATIONS

References (51–61) appear in the Supplementary Material.

REFERENCES

1. Liu, X.-A., V. Rizzo, and S. Puthanveettil, 2012. Pathologies of axonal transport in neurodegenerative diseases. *J Transl Neurosci* 3:355–372.

2. Millecamps, S., and J.-P. Julien, 2013. Axonal transport deficits and neurodegenerative diseases. *Nat Rev Neurosci* 14:161.

3. Smith, B. N., S. D. Topp, C. Fallini, H. Shibata, H.-J. Chen, C. Troakes, A. King, N. Ticozzi, K. P. Kenna, A. Soragia-Gkazi, et al., 2017. Mutations in the vesicular trafficking protein annexin A11 are associated with amyotrophic lateral sclerosis. *Science translational medicine* 9:eaad9157.

4. Kardon, J. R., and R. D. Vale, 2009. Regulators of the cytoplasmic dynein motor. *Nat Rev Mol Cell Bio* 10:854.

5. Fu, M.-m., and E. L. Holzbaur, 2014. Integrated regulation of motor-driven organelle transport by scaffolding proteins. *Trends Cell Biol* 24:564–574.

6. Cianfrocco, M. A., M. E. DeSantis, A. E. Leschziner, and S. L. Reck-Peterson, 2015. Mechanism and regulation of cytoplasmic dynein. *Annu Rev Cell Dev Bi* 31:83–108.

7. Higuchi, Y., P. Ashwin, Y. Roger, and G. Steinberg, 2014. Early endosome motility spatially organizes polysome distribution. *J Cell Biol* 204:343–357.

8. Baumann, S., J. König, J. Koepke, and M. Feldbrügge, 2014. Endosomal transport of septin mRNA and protein indicates local translation on endosomes and is required for correct septin filamentation. *Embo Rep* 15:94–102.

9. Baumann, S., T. Pohlmann, M. Jungbluth, A. Brachmann, and M. Feldbrügge, 2012. Kinesin-3 and dynein mediate microtubule-dependent co-transport of mRNPs and endosomes. *J Cell Sci* 125:2740–2752.

10. Pohlmann, T., S. Baumann, C. Haag, M. Albrecht, and M. Feldbrügge, 2015. A FYVE zinc finger domain protein specifically links mRNA transport to endosome trafficking. *Elife* 4:e06041.

11. Schmid, M., A. Jaedicke, T.-G. Du, and R.-P. Jansen, 2006. Coordination of endoplasmic reticulum and mRNA localization to the yeast bud. *Curr Biol* 16:1538–1543.

12. Guimaraes, S. C., M. Schuster, E. Bielska, G. Dagdas, S. Kilaru, B. R. Meadows, M. Schrader, and G. Steinberg, 2015. Peroxisomes, lipid droplets, and endoplasmic reticulum "hitchhike" on motile early endosomes. *J Cell Biol* 211:945–954.

13. Salogiannis, J., M. J. Egan, and S. L. Reck-Peterson, 2016. Peroxisomes move by hitchhiking on early endosomes using the novel linker protein PxdA. *J Cell Biol* 201512020.

14. Lin, C., M. Schuster, S. C. Guimaraes, P. Ashwin, M. Schrader, J. Metz, C. Hacker, S. J. Gurr, and G. Steinberg, 2016. Active diffusion and microtubule-based transport oppose myosin forces to position organelles in cells. *Nature communications* 7:11814.

15. Liao, Y.-C., M. Fernandopulle, G. Wang, H. Choi, L. Hao, C. M. Drerup, S. Qamar, J. Nixon-Abell, Y. Shen, W. Meadows, et al., 2019. RNA granules hitchhike on lysosomes for long-distance transport, using annexin A11 as a molecular tether. *Cell* 179:147–164.

16. Salogiannis, J., and S. L. Reck-Peterson, 2017. Hitchhiking: a non-canonical mode of microtubule-based transport. *Trends Cell Biol* 27:141–150.

17. Ando, D., N. Korabel, K. C. Huang, and A. Gopinathan, 2015. Cytoskeletal network morphology regulates intracellular transport dynamics. *Biophys J* 109:1574–1582.

18. Godec, A., and R. Metzler, 2015. Signal focusing through active transport. *Phys Rev E* 92:010701.

19. Mogre, S. S., and E. F. Koslover, 2018. Multimodal transport and dispersion of organelles in narrow tubular cells. *Phys Rev E* 97:042402.

20. Müller, M. J., S. Klumpp, and R. Lipowsky, 2008. Tug-of-war as a cooperative mechanism for bidirectional cargo transport by molecular motors. *Proceedings of the National Academy of Sciences* 105:4609–4614.

21. Ross, J. L., M. Y. Ali, and D. M. Warshaw, 2008. Cargo transport: molecular motors navigate a complex cytoskeleton. *Curr Opin Cell Biol* 20:41–47.

22. Bergman, J. P., M. J. Bovyn, F. F. Doval, A. Sharma, M. V. Gudheti, S. P. Gross, J. F. Allard, and M. D. Vershinin, 2018. Cargo navigation across 3D microtubule intersections. *P Natl Acad Sci* 115:537–542.

23. Bharti, P., W. Schliebs, T. Schievelbusch, A. Neuhaus, C. David, K. Kock, C. Herrmann, H. E. Meyer, S. Wiese, B. Warscheid, et al., 2011. PEX14 is required for microtubule-based peroxisome motility in human cells. *J Cell Sci* 124:1759–1768.

24. Schwarz, T. L., 2013. Mitochondrial trafficking in neurons. *Cold Spring Harbor perspectives in biology* 5:a011304.

25. Kang, J.-S., J.-H. Tian, P.-Y. Pan, P. Zald, C. Li, C. Deng, and Z.-H. Sheng, 2008. Docking of axonal mitochondria by syntaphilin controls their mobility and affects short-term facilitation. *Cell* 132:137–148.

26. Agrawal, A., G. Pekkurnaz, and E. F. Koslover, 2018. Spatial control of neuronal metabolism through glucose-mediated mitochondrial transport regulation. *Elife* 7:e40986.

27. Pekkurnaz, G., J. C. Trinidad, X. Wang, D. Kong, and T. L. Schwarz, 2014. Glucose regulates mitochondrial motility via Milton modification by O-GlcNAc transferase. *Cell* 158:54–68.

28. Barlan, K., and V. I. Gelfand, 2017. Microtubule-based transport and the distribution, tethering, and organization of organelles. *Cold Spring Harbor perspectives in biology* 9:a025817.

29. Egan, M. J., M. A. McClintock, and S. L. Reck-Peterson, 2012. Microtubule-based transport in filamentous fungi. *Curr Opin Microbiol* 15:637–645.

30. Meijer, W. H., L. Gidijala, S. Fekken, J. A. Kiel, M. A. van den Berg, R. Lascaris, R. A. Bovenberg, and I. J. van der Klei, 2010. Peroxisomes are required for efficient penicillin biosynthesis in Penicillium chrysogenum. *Appl. Environ. Microbiol.* 76:5702–5709.

31. Mussel, M., K. Zeevy, H. Diamant, and U. Nevo, 2014. Drag of the cytosol as a transport mechanism in neurons. *Biophysical journal* 106:2710–2719.

32. Brangwynne, C. P., F. MacKintosh, and D. A. Weitz, 2007. Force fluctuations and polymerization dynamics of intracellular microtubules. *P Natl Acad Sci* 104:16128–16133.

33. Koslover, E. F., and A. J. Spakowitz, 2014. Multiscale dynamics of semiflexible polymers from a universal coarse-graining procedure. *Phys Rev E* 90:013304.

34. Kratky, O., and G. Porod, 1949. Röntgenuntersuchung gelöster fadenmoleküle. *Recl Trav Chim Pay-b* 68:1106–1122.

35. Spakowitz, A. J., and Z.-G. Wang, 2005. End-to-end distance vector distribution with fixed end orientations for the wormlike chain model. *Phys Rev E* 72:041802.

36. Stine, R., 1989. An introduction to bootstrap methods: Examples and ideas. *Sociol Method Res* 18:243–291.

37. Broedersz, C. P., and F. C. MacKintosh, 2014. Modeling semiflexible polymer networks. *Rev Mod Phys* 86:995.

38. Berg, H. C., and E. M. Purcell, 1977. Physics of chemoreception. *Biophys J* 20:193–219.

39. Hvidt, S., F. H. M. Nestler, M. L. Greaser, and J. D. Ferry, 1982. Flexibility of myosin rod determined from dilute solution viscoelastic measurements. *Biochemistry-us* 21:4064–4073.

40. Phillips Jr, G. N., and S. Chacko, 1996. Mechanical properties of tropomyosin and implications for muscle regulation. *Biopolymers* 38:89–95.

41. Wolgemuth, C. W., and S. X. Sun, 2006. Elasticity of α-helical coiled coils. *Phys Rev Lett* 97:248101.

42. van Noort, J., T. van der Heijden, M. de Jager, C. Wyman, R. Kanaar, and C. Dekker, 2003. The coiled-coil of the human Rad50 DNA repair protein contains specific segments of increased flexibility. *P Natl Acad Sci* 100:7581–7586.

43. Wang, X., and T. L. Schwarz, 2009. The mechanism of Ca2+-dependent regulation of kinesin-mediated mitochondrial motility. *Cell* 136:163–174.

44. Wu, X. S., K. Rao, H. Zhang, F. Wang, J. R. Sellers, L. E. Matesic, N. G. Copeland, N. A. Jenkins, and J. A. Hammer III, 2002. Identification of an organelle receptor for myosin-Va. *Nat Cell Biol* 4:271.

45. Chen, K., B. Wang, J. Guan, and S. Granick, 2013. Diagnosing heterogeneous dynamics in single-molecule/particle trajectories with multiscale wavelets. *Acs Nano* 7:8634–8644.

46. Bálint, Š., I. V. Vilanova, Á. S. Álvarez, and M. Lakadamyali, 2013. Correlative live-cell and super-resolution microscopy reveals cargo transport dynamics at microtubule intersections. *Proceedings of the National Academy of Sciences* 110:3375–3380.

47. Verdeny-Vilanova, I., F. Wehnekamp, N. Mohan, Á. S. Álvarez, J. S. Borbely, J. J. Otterstrom, D. C. Lamb, and M. Lakadamyali, 2017. 3D motion of vesicles along microtubules helps them to circumvent obstacles in cells. *J Cell Sci* 130:1904–1916.

48. Hancock, W. O., 2014. Bidirectional cargo transport: moving beyond tug of war. *Nature reviews Molecular cell biology* 15:615–628.

49. Zajac, A. L., Y. E. Goldman, E. L. Holzbaur, and E. M. Ostap, 2013. Local cytoskeletal and organelle interactions impact molecular-motor-driven early endosomal trafficking. *Current Biology* 23:1173–1180.

50. Lakadamyali, M., 2014. Navigating the cell: how motors overcome roadblocks and traffic jams to efficiently transport cargo. *Physical Chemistry Chemical Physics* 16:5907–5916.

51. Szewczyk, E., T. Nayak, C. E. Oakley, H. Edgerton, Y. Xiong, N. Taheri-Talesh, S. A. Osmani, and B. R. Oakley, 2006. Fusion PCR and gene targeting in Aspergillus nidulans. *Nat Protoc* 1:3111.

52. Nayak, T., E. Szewczyk, C. E. Oakley, A. Osmani, L. Ukil, S. L. Murray, M. J. Hynes, S. A. Osmani, and B. R. Oakley, 2006. A versatile and efficient gene-targeting system for Aspergillus nidulans. *Genetics* 172:1557–1566.

53. Todd, R. B., M. A. Davis, and M. J. Hynes, 2007. Genetic manipulation of Aspergillus nidulans: meiotic progeny for genetic analysis and strain construction. *Nat Protoc* 2:811.

54. Waring, R. B., G. S. May, and N. R. Morris, 1989. Characterization of an inducible expression system in Aspergillus nidulans using alcA and tubulincoding genes. *Gene* 79:119–130.

55. Gibson, D. G., L. Young, R.-Y. Chuang, J. C. Venter, C. A. Hutchison III, and H. O. Smith, 2009. Enzymatic assembly of DNA molecules up to several hundred kilobases. *Nat Methods* 6:343.

56. Chen, B.-C., W. R. Legant, K. Wang, L. Shao, D. E. Milkie, M. W. Davidson, C. Janetopoulos, X. S. Wu, J. A. Hammer, Z. Liu, et al., 2014. Lattice light-sheet microscopy: imaging molecules to embryos at high spatiotemporal resolution. *Science* 346:1257998.

57. Schindelin, J., I. Arganda-Carreras, E. Frise, V. Kaynig, M. Longair, T. Pietzsch, S. Preibisch, C. Rueden, S. Saalfeld, B. Schmid, et al., 2012. Fiji: an open-source platform for biological-image analysis. *Nat Methods* 9:676.

58. Schneider, C. A., W. S. Rasband, and K. W. Eliceiri, 2012. NIH Image to ImageJ: 25 years of image analysis. *Nat Methods* 9:671.

59. Crocker, J. C., and D. G. Grier, 1996. Methods of digital video microscopy for colloidal studies. *J Colloid Interf Sci* 179:298–310.

60. Gao, Yongxiang and Kilfoil, Maria. MATLAB 3D feature-finding algorithms. downloaded from http://people.umass.edu/kilfoil/downloads.html.

61. Smith, J. J., and J. D. Aitchison, 2013. Peroxisomes take shape. *Nat Rev Mol Cell Bio* 14:803.